# NJC

Accepted Manuscript


This is an *Accepted Manuscript*, which has been through the Royal Society of Chemistry peer review process and has been accepted for publication.

*Accepted Manuscripts* are published online shortly after acceptance, before technical editing, formatting and proof reading. Using this free service, authors can make their results available to the community, in citable form, before we publish the edited article. We will replace this *Accepted Manuscript* with the edited and formatted *Advance Article* as soon as it is available.

You can find more information about *Accepted Manuscripts* in the Information for Authors.

Please note that technical editing may introduce minor changes to the text and/or graphics, which may alter content. The journal's standard Terms & Conditions and the Ethical guidelines still apply. In no event shall the Royal Society of Chemistry be held responsible for any errors or omissions in this *Accepted Manuscript* or any consequences arising from the use of any information it contains.

ROYAL SOCIETY OF CHEMISTRY

www.rsc.org/njc

NJC

RSCPublishing

LETTER

# Amorphous Nickel-Cobalt-Boron alloy as advanced pseudocapacitor material

Cite this: DOI: 10.1039/c3nj00000x

Wei Zhang,[a] Xiuli Zhang,[b] Yueyue Tan,[a] Jianxiang Wu,[a] Yilong Gao,[a] Bohejin Tang,[a#] and Yuanci Wang[a]

Received 00th XXXXX 2013,
Accepted 00th XXXXX 2013

DOI: 10.1039/c3nj00000x

www.rsc.org/njc

**Abstract: The nanoparticles of amorphous Nickel-Cobalt-Boron alloy powder, prepared by chemical reduction, show superior specific capacitance when used as pseudocapacitor material. The amorphous Nickel-Cobalt-Boron alloy exhibits a noticeable pseudocapacitance with 1310 F $g^{-1}$ at 1.5 A $g^{-1}$ in the electrolyte of 6 M KOH.**

Electrochemical capacitors (ECs) are mainly classified as electrical double layer capacitors (EDLCs) and pseudocapacitors[1, 2]. Currently, commercial EDLC devices are mainly electric double layer capacitors (EDLCs) using two symmetric high surface-area activated carbon (AC) electrodes in organic electrolytes. The specific capacitance for high surface area activated-carbon is about 100 F $g^{-1}$ in aqueous electrolytes. However, to create a viable energy storage device for a hybrid vehicle, it is important to increase the energy storage capacity of existing double layer capacitors. This may be achieved by a concept called pseudocapacitance[3] that not only develops the typical double layer capacitance, but also exhibits pseudocapacitance due to surface redox couples providing net charge transfer. Transition metal oxides and hydroxides, such as $RuO_2$ (720 F $g^{-1}$), $Fe_3O_4$ (135 F $g^{-1}$), $Co_3O_4$( 358 F $g^{-1}$) , $MnO_2$ (120 F $g^{-1}$), $Ni(OH)_2$ (400 F $g^{-1}$) etc.[4-8], are promising pseudocapacitive materials because they possess a variety of reversible oxidation states for highly efficient redox charge transfer. However, the exploration of electrode materials with higher power performance and low cost for pseudo capacitors is still of great importance.

Amorphous alloys are metastable and, as prepared, they usually exhibit a high degree of compositional as well as topological disorder. Indeed, the occurrence of very large concentrations of compositional disorder may be possible in certain alloy systems only when they are put in an amorphous state. Up to now, a large number of M-B amorphous alloys have been synthesized by varying the metal ions (Ni, Co, Fe, Ru etc.), mainly by direct chemical reduction of metallic ions with borohydride[9-11]. They have been widely studied in catalytic reaction owing to their higher activity, and better selectivity[12]. However, we rarely discover this material applied in pseudo capacitors. In the previous report, we had research the nanoparticles of amorphous Ni–B and Ni–Mn–B alloys as electrochemical pseudocapacitor materials for potential energy storage applications[13]. The specific capacitance of Ni–B and Ni–Mn–B electrodes are observed to be 562 and 768 F $g^{-1}$, respectively. The capacitance of amorphous Ni-B alloy is higher than the crystalline Ni (416.6 F $g^{-1}$), which is prepared successfully through reducing nickel chloride by hydrazine hydrate[14]. We also find that Wang et al.[15] reported that the ultrafine amorphous alloy powders (UAAP) of Fe-B and Co-B were synthesized and tested for possible use as electroactive anodic materials. The experimental results

demonstrated that the Co−B particles so prepared show excellent electrochemical reversibility and considerably high charge−discharge capacity. Liu et al.[16] had prepared a series of $Co_xB$ (x = 1, 2, 3) alloys by arc melting. The electrochemical experimental results demonstrated that the $Co_xB$ (x = 1, 2, 3) series alloys showed excellent cycling stability. Through previous researches, we tried to take the nature advantages of amorphous alloy and apply the materials for pseudocapacitors, hoping to break through in the special capacitance.

In this paper, amorphous Nickel-Cobalt-Boron alloy powder was evaluated as a possible candidate electrode material for pseudocapacitor using different techniques including cyclic voltammetry, electrochemical impedance spectroscopy and galvanostatic charge and discharge. The high specific capacitance and remarkable rate capability are promising for applications in pseudocapacitors with both high energy and power densities.

The chemical composition of the sample, analyzed by an inductively coupled plasma (ICP) method, was found to be $Ni_{47.5}Co_{20.4}B_{32.1}$. It is almost the same as the initial Ni/Co ratio of 7: 3 in the chemical preparation. Chen[17] suggested that the following reactions would occur to formx Ni-Co-B during the reduction by $NaBH_4$:

$$BH_4^- + 2H_2O \longrightarrow BO_2^- + 4H_2 \quad (1)$$

$$2Ni^{2+} + BH_4^- + 2H_2O \longrightarrow 2Ni + BO_2^- + 4H^+ + 2H_2 \quad (2)$$

$$2Co^{2+} + BH_4^- + 2H_2O \longrightarrow 2Co + BO_2^- + 4H^+ + 2H_2 \quad (3)$$

$$BH_4^- + H_2O \longrightarrow B + OH^- + 2.5H_2 \quad (4)$$

These reactions include the reduction of nickel and cobalt ions ((2) and (3)), the reduction of borohydride ion (4) and the hydrolysis of borohydride (1). The relative rates of the reduction reactions of (2), (3) and (4) would manipulate the formation of Ni-Co-B and influence their electrochemical propertise. As it is shown in Fig. 1a, the SEM morphology of Ni-Co-B demonstrates short-range ordering, which is in good agreement with the literature report[18]. The disordered amorphous Ni-Co-B alloy constructed a great deal of cavities or microstructures. Its unique porous structure gave more electrochemical capacitance.The specific surface area of the powders was determined by the BET method. The base Ni-Co-B has a surface area of 27.4 $m^2 g^{-1}$, which is almost the same as that of reported Ni-Co-B[19, 20]. It can be seen from the TEM image (Fig. 1b) of the Ni-Co-B particles prepared in this work. It can be clearly visualized that the Ni-Co-B powers consisting of small grains of 60-80 nm size and each grain is composed of very fine particles. The amorphous characteristics of the Ni-Co-B could be further confirmed by selected area electron diffraction (SAED), which shows a broad and featureless diffraction ring, suggesting a amorphous structure of the powders. A single broad peak around 2θ= 45ºin the pattern indicates the amorphous phase of the prepared sample (Fig. 2), consistent in literature[20, 21].

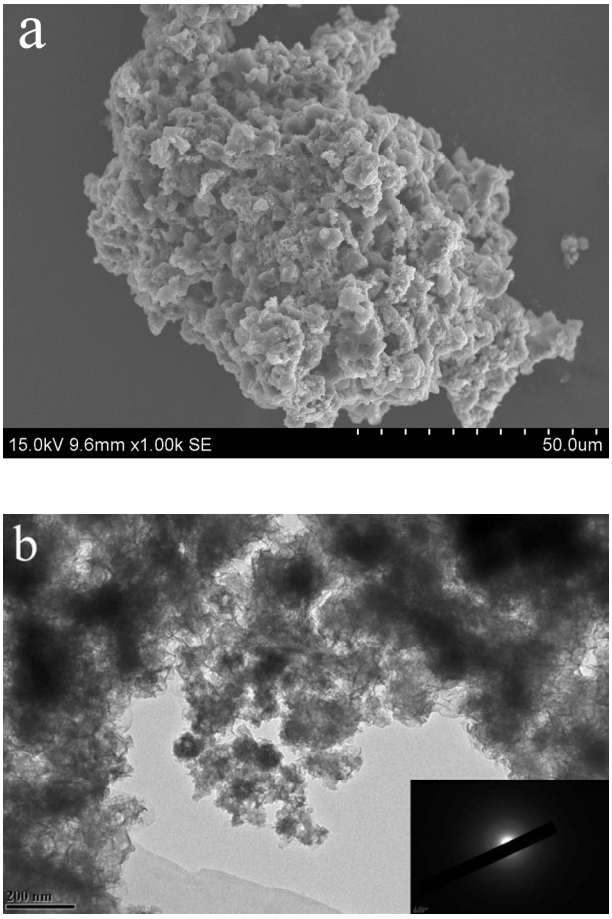


Fig. 1 (a). SEM morphology of the Ni-Co-B . (b) The TEM micrograph and SAED of Ni-Co-B.

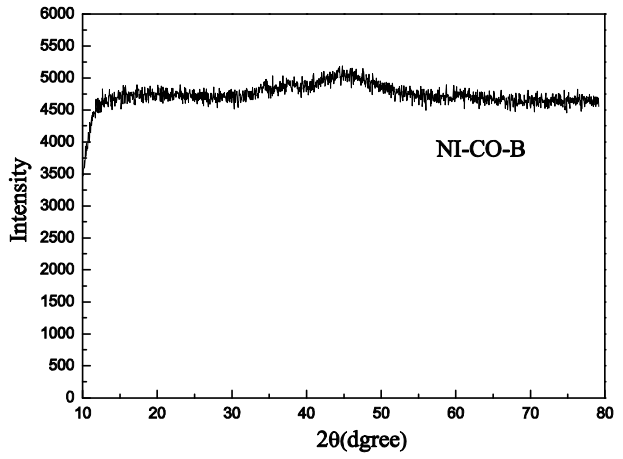


Fig. 2. XRD patterns of the Ni-Co-B.

Figure 3a shows the cyclic voltammetry (CV) curves of Ni-Co-B in 6 M KOH solution at a scanning rate of 5,10,20,30 and 40mV/s, respectively. A pair of well-defined redox peaks at 0 V and 0.25 V can be clearly observed in the CV curves, particularly at the low scan rate (see the inset of Figure 3a). With the scan rate increasing, the oxidation peaks shift to right while the reduction peaks shift to left, suggesting that the redox reversibility of the hybrid electrode is kinetically associated with a rate-controlling process[22, 23].

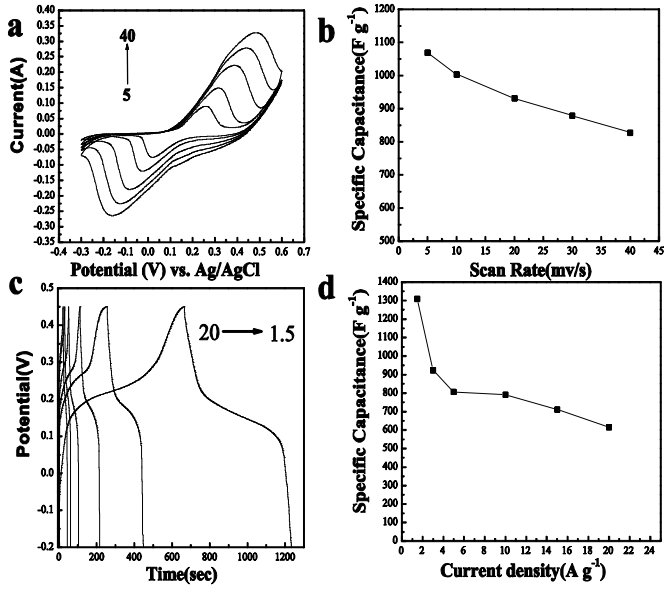


Fig. 3. (a) The cyclic voltammetry curves of Ni-Co-B (3.0 mg) at an increasing voltage scanning rate of 5, 10, 20,30 and 40 mV $s^{-1}$; (b) The specific capacitance of Ni-Co-B at different scan rates; (c) The charge-discharge curves of Ni-Co-B at a different current density. (d) The specific capacitance of Ni-Co-B at various discharge current densities.

From the CV, the specific capacitance can be estimated as follows[24]:

$$C = \frac{1}{2 \times v \times \Delta m \times \Delta V} \int I \, dV$$

Where $C$ is the specific capacitance (F $g^{-1}$), $v$ is the scan rate (V/s), $\Delta m$ is the mass of the active material (g), $\Delta V$ is the potential window (V) and $I\,dV$ represents the area under CV curve (Q). All specific capacitance data with various scan rates are collected in Fig. 3b. It is noteworthy that the Ni-Co-B as high as 1070 F $g^{-1}$ has been obtained at a scan rate of 5 mV $s^{-1}$ and the Ni-Co-B of 827 F $g^{-1}$ was obtained even at a high scan rate of 40 mV $s^{-1}$.The specific capacitance is decreased with increase in the scan rate. It indicates that the active material at the inner surface does not get fully involved in the electrochemical process, which is due to the limited ion diffusion [25].On the other hand, the ions from electrolyte can access to almost all available sites of the electrode at a low scan rate, leading to a complete insertion reaction, and thus resulting in a higher specific capacitance.

Galvanostatic charge/discharge measurement of Ni-Co-B electrode was carried out in a 6 M KOH solution between -0.2 and 0.45 V at a current density of 1.5 A $g^{-1}$. As illustrated in Fig. 3c, the nonlinear charging/discharging profile indicate a significant contribution of pseudocapacitance from amorphous Ni-Co-B alloy. The specific capacitance can be calculated from the galvanostatic charge-discharge curve according to equation[26]:

$$C = \frac{I \times \Delta t}{\Delta V \times \Delta m}$$

where $C$ is the specific capacitance (F $g^{-1}$), $I$ is the current (A), $\Delta t$ is the discharge time(sec), $\Delta V$ is the potential window (V) and $\Delta m$ is mass of the electroactive material(g). As shown in Fig. 3d, the specific capacitance calculated from these galvanostatic charge/discharge curves is 1310 F $g^{-1}$ at current densities of 1.5 A $g^{-1}$, which is also

the highest capacitance among the other stoichiometry samples of Ni-Co-B. The results also show the decrease of specific capacitance with the increment of current density. However, the pseudocapacitors exhibit high rate capability due to the specific capacitance at current density of 20 A $g^{-1}$ maintaining 47% retention of that measured at initial current density of 1.5 A $g^{-1}$, which is attributed to high rate performance of Ni-Co-B.

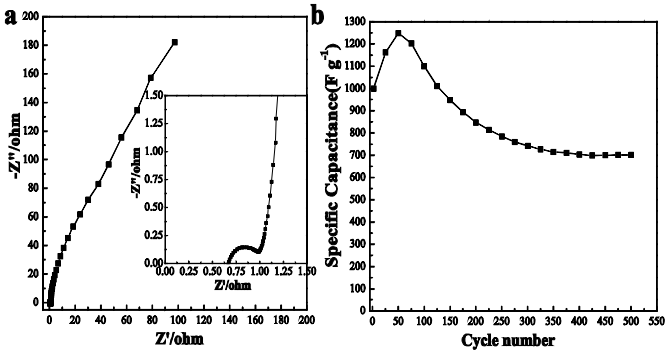


Fig. 4. (a) Nyquist curve of Ni-Co-B ( inset is the magnification of Nyquist curve); (b) The normalized capacitance of Ni-Co-B (3.3mg) taken from cyclic voltammetry curves. Z' is real impedance. Z'' is imaginary impedance.

To get more information on conductive performance of the sample Ni-Co-B electrode, electrochemical impedance spectroscopy (EIS) measurements were performed. As shown in Fig. 4a, Nyquist plot exhibits a single semi-circle in the high-frequency region and a straight line in the low-frequency region. The semicircle should be attributed to the charge transfer process at electrode/electrolyte interface, and the straight line should be ascribed to the diffusion process in the solid. The slope close to 45º along the imaginary axis (Z'') at low frequencies is due to a Warburg impedance (a limiting diffusion process), and is not useful for charge storage. The electrode resistance was observed for Ni-Co-B, which was close to 0.6 Ω. This shows that the electrode in the present study was of a highly conducting nature. In order to investigate the cycling performance, the cyclic voltammetry test was carried out up to 500 cycles at a scan rate of 10 mV $s^{-1}$ and the calculated specific capacitance is given in Fig. 4b. The specific capacitance gradually increased up to 50 cycles and then it started to decrease until the steady trend. The gradual increase in specific capacitance during the initial cycling may be ascribed to activation of the electrode, as electrolytes in general require a certain period of time to penetrate the entire inner space of an active electrode material[27]. However, it still retains a capacity of 650 F $g^{-1}$ after 500 cycles, reflecting the good long-term cyclability of Ni-Co-B.

In summary, nanoparticles of amorphous Ni-Co-B alloy were prepared by chemical reduction. Characterization by XRD and TEM showed that it has a typical amorphous alloy structure with the particle size from 60 to 80 nm. The electrochemical tests show that the pseudocapacitor exhibits good electrochemical capacitance performance, excellent discharge rate, highly conducting nature and good stability. The specific capacitance value of Ni-Co-B is 1310 F $g^{-1}$ in 6 M KOH at a current density of 1.5 A $g^{-1}$. The amorphous Ni-Co-B (molar ratio nickel sulfate: cobalt chloride = 7:3) alloy is the most significant part in our work. The other amorphous Ni-Co-B alloy of different molar ratio will be discussed and published in full text. Combined with the advantages of low cost, easy operation and environmentally friendly nature, this amorphous Ni-Co-B alloy electrode shows great promise for applications in commercial high-capacity pseudocapacitors.

## Experimental

### Material Synthesis

A typical experimental procedure is as follows: 50 mL of sodium borohydride solution (0.18 mol $L^{-1}$) was first prepared and adjusted to pH 12 with sodium hydroxide to prevent violent hydrolysis. The 3 mmol of metallic salt (molar ratio nickel sulfate: cobalt chloride = 7:3) was dissolved in 5ml of deionized water and then cooled in an ice bath. The chemical reduction reaction was carried out by adding borohydride solution dropwise into metal salt solution while being stirred. When the addition was complete, the solution bath was continually stirred for about 1h to release the hydrogen and to prevent burning of the precipitate following filtration and all the reaction was performed under $N_2$ atmosphere. After that, the precipitate was washed with distilled water three times, followed by ethanol three times. Finally, the sample was stored in absolute ethanol until the time of use (denoted as Ni-Co-B).



 

All the reagents were of analytical grade and used as received without further purification (Shanghai Chemical Reagent Company).

Electrochemical measurements

The working electrode was prepared by mixing Ni-Co-B material, acetylene black and poly tetrafluoroethylene (PTFE) binder with the weight percent ratio of 75:20:5 with small amount of ethanol. When it was dispersed in alcohol and the mixtures was pressed onto nickel foams, which was then dried at 90°C in vacuum. The geometric surface area of the prepared working electrode is 1 $cm^2$, and then the electrodes were pressed at a pressure of 12 MPa. Nickel foam (1.6 mm thick, 95% purity, Goodfellow) was used as a current collector.

Electrochemical properties and capacitance measurements were performed by the three-electrode configuration. The testing system consists of a working electrode, a platinum sheet as a counter electrode and an Ag/AgCl electrode as the reference electrode in a 6 M KOH solution. Cyclic voltammetry, constant current charge/discharge and impedance were performed on a CHI660D instrument in the potential range of -0.3-0.6 V with varied scan rates from 5 to 40 mV $s^{-1}$. All the experiments were done three times to ensure accuracy.

Compositional and Structural Characterization

The powder X-ray diffractions (PXRD) of the samples were performed on a diffraction meter (D/Max-RB) with Cu-Kα radiation (λ=1.54056 Å ) and a graphite monochromator at 50 kV, 100 mA. The chemical composition of Ni-Co-B alloy powder was analyzed by inductively coupled plasma (ICP, Prodigy, Leeman).The size and morphological view of the alloy powders were observed by a transmission electron microscope (TEM) on Hitachi H-800 microscope. Scanning electron micrographs (SEM) analysis (HITACHI S-3400N) was used to capture and determine the morphologies of the sample. $N_2$ adsorption–desorption isotherms were measured using a Micromeritics ASAP2460 analyzer at 77 K; The Brunauer-Emmett-Teller (BET) method was utilized to calculate the specific surface areas.

## Acknowledgements

This work is supported by Natural Science Foundation of Shanghai (Contract No. 13ZR1418200).

## Notes and references

*a College of Chemistry and Chemical Engineering, Shanghai University of Engineering Science, Shanghai 201620, PR China*

*b School of Fundamental Studies, Shanghai University of Engineering Science, Shanghai 201620, PR China*

*E-mail: tangbohejin@sues.edu.cn*

1. L. Yang, S. Cheng, Y. Ding, X. Zhu, Z. L. Wang and M. Liu, *Nano Lett.*, 2011, 12, 321-325.
2. J. E. Nerz, S. Prasad and G. Thomas, Google Patents, 1995.
3. H. Wang, H. S. Casalongue, Y. Liang and H. Dai, *J. Am. Chem. Soc.*, 2010, 132, 7472-7477.
4. J. Mu, B. Chen, Z. Guo, M. Zhang, Z. Zhang, P. Zhang, C. Shao and Y. Liu, *Nanoscale*, 2011, 3, 5034-5040.
5. C. M. Ghimbeu, A. Malak-Polaczyk, E. Frackowiak and C. Vix-Guterl, *J. Appl. Electrochem.*, 2014, 44, 123-132.
6. X.-H. Xia, J.-P. Tu, X.-L. Wang, C.-D. Gu and X.-B. Zhao, *Chem. Commun.*, 2011, 47, 5786-5788.
7. U. Patil, K. Gurav, V. Fulari, C. Lokhande and O. S. Joo, *J. Power Sources*, 2009, 188, 338-342.
8. J. Zheng, P. Cygan and T. Jow, *J. Electrochem. Soc.*, 1995, 142, 2699-2703.
9. H. Li, D. Chu, J. Liu, M. Qiao, W. Dai and H. Li, *Adv. Synth. Catal.*, 2008, 350, 829-836.
10. Y. Wang, X. Ai, Y. Cao and H. Yang, *Electrochem. Commun.*, 2004, 6, 780-784.
11. H. Li, D. Zhang, G. Li, Y. Xu, Y. Lu and H. Li, *Chem. Commun.*, 2010, 46, 791-793.
12. J.-F. Deng, H. Li and W. Wang, *Catal. Today*, 1999, 51, 113-125.
13. W. Zhang, Y. Tan, Y. Gao, J. Wu, B. Tang and J. Zhao, *RSC Advances*, 2014, 4, 27800-27804.
14. X. Wu, W. Xing, L. Zhang, S. Zhuo, J. Zhou, G. Wang and S. Qiao, *Powder Technol.*, 2012, 224, 162-167.

15. Y. D. Wang, X. P. Ai and H. X. Yang, *Chem. Mater.*, 2004, 16, 5194-5197.
16. Y. Liu, Y. Wang, L. Xiao, D. Song, Y. Wang, L. Jiao and H. Yuan, *Electrochim. Acta*, 2008, 53, 2265-2271.
17. Y. Chen, *Catal. Today*, 1998, 44, 3-16.
18. J. Ingersoll, N. Mani, J. Thenmozhiyal and A. Muthaiah, *J. Power Sources*, 2007, 173, 450-457.
19. H. Luo, H. Li and L. Zhuang, *Chemistry Letters*, 2001, 404-405.
20. J.-H. Shen and Y.-W. Chen, *Journal of Molecular Catalysis A: Chemical*, 2007, 273, 265-276.
21. M.-H. Lin, B. Zhao and Y.-W. Chen, *Ind. Eng. Chem. Res.*, 2009, 48, 7037-7043.
22. J. Yan, Z. Fan, W. Sun, G. Ning, T. Wei, Q. Zhang, R. Zhang, L. Zhi and F. Wei, *Adv. Funct. Mater.*, 2012, 22, 2632-2641.
23. M. Hasan, M. Jamal and K. M. Razeeb, *Electrochim. Acta*, 2012, 60, 193-200.
24. V. Nithya, R. Kalai Selvan, D. Kalpana, L. Vasylechko and C. Sanjeeviraja, *Electrochim. Acta*, 2013, 109, 720-731.
25. R. K. Sharma, H.-S. Oh, Y.-G. Shul and H. Kim, *Physica B: Condensed Matter*, 2008, 403, 1763-1769.
26. B. Hu, X. Qin, A. M. Asiri, K. A. Alamry, A. O. Al-Youbi and X. Sun, *Electrochim. Acta*, 2013, 107, 339-342.
27. X.-C. Dong, H. Xu, X.-W. Wang, Y.-X. Huang, M. B. Chan-Park, H. Zhang, L.-H. Wang, W. Huang and P. Chen, *ACS Nano*, 2012, 6, 3206-3213.



 